# Fractional quantum Hall edge: Effect of nonlinear dispersion and edge roton

Shivakumar Jolad,[1] Diptiman Sen,[2] and Jainendra K. Jain[1,3]
[1]*Department of Physics, Pennsylvania State University, University Park, Pennsylvania 16802, USA*
[2]*Center for High Energy Physics, Indian Institute of Science, Bangalore 560012, India*
[3]*Department of Theoretical Physics, Tata Institute of Fundamental Research, Homi Bhabha Road, Colaba, Mumbai 400005, India*
(Received 22 May 2010; revised manuscript received 22 July 2010; published 13 August 2010)

According to Wen's theory, a universal behavior of the fractional quantum Hall edge is expected at sufficiently low energies, where the dispersion of the elementary edge excitation is linear. A microscopic calculation shows that the actual dispersion is indeed linear at low energies, but deviates from linearity beyond certain energy, and also exhibits an "edge roton minimum." We determine the edge exponent from a microscopic approach, and find that the nonlinearity of the dispersion makes a surprisingly small correction to the edge exponent even at energies higher than the roton energy. We explain this insensitivity as arising from the fact that the energy at maximum spectral weight continues to show an almost linear behavior up to fairly high energies. We also study, in an effective-field theory, how interactions modify the exponent for a reconstructed edge with multiple edge modes. Relevance to experiment is discussed.

DOI: 10.1103/PhysRevB.82.075315 PACS number(s): 73.43.−f, 71.10.Pm

## I. INTRODUCTION

The edge of a fractional quantum Hall (FQH) system[1] constitutes a realization of a chiral Tomonaga-Luttinger liquid (CTLL). (The word chiral implies that all the fermions move in the same direction.) In a seminal work, Wen[2,3] postulated that the CTLL at the FQH edge is very special in that the exponent characterizing its long-distance, low-energy physics is a universal quantized number, which depends only on the quantized Hall conductance of the bulk state but not on other details. He described the FQH edge through an effective-field theory approach (EFTA) based on the postulate that the electron operator at the edge of the $\nu=1/m$ FQH state has the form

$$\hat{\psi}(x) \sim e^{-i\sqrt{m}\hat{\phi}(x)}, \tag{1}$$

where $\hat{\phi}(x)$ is the bosonic field operator. The imposition of antisymmetry forces $m$ to be an odd integer,[2] which, in turn, leads to quantized exponents for various correlation functions. In particular, it predicts a relation $I \sim V^3$ between the current ($I$) and the voltage ($V$) for tunneling from a three-dimensional Fermi liquid into the 1/3 FQH edge, which has been tested experimentally by Chang *et al.* and Grayson *et al.*[4–8]

Wen's theory describes the FQHE edge in the asymptotic limit of low energies and long distances. The CTLL description is inapplicable at energies comparable to or larger than the bulk gap, where bulk excitations become available; we will not consider such high energies in this work. However, even in a range of energies below the bulk gap, deviations from the ideal asymptotic behavior may arise because the dispersion of the elementary edge excitation deviates from linearity and also exhibits an "edge roton minimum." The aim of this paper is to estimate these corrections from a microscopic approach. To focus on these corrections, we make appropriate approximations [mainly a neglect of composite fermion (CF) $\Lambda$ level mixing, discussed previously in this context[9]] that guarantee an ideal quantized behavior at very low energies.

A deviation from linearity in the dispersion of the elementary edge excitation is expected to produce corrections for the following reason. In the bosonic model of edge excitations, the spectral weights of all excitations at a given momentum obey a sum rule [see Eq. (20)], first demonstrated by Palacios and MacDonald,[10] which is valid up to a unitary rotation of the basis. The long-time behavior of the Green's function and the differential conductance for tunneling from an external Fermi liquid into the FQH edge, on the other hand, are sensitive to the states within an energy slice. However, for linear dispersion, the energy and momentum are uniquely related, so the sum rule is also valid for all states at a given *energy*, which produces a quantized power law exponent for the differential conductance. (A more detailed discussion is given in Appendix). A nonlinearity in the dispersion, on the other hand, produces an energy band for excitations, as shown, for example, in Fig. 5. In the absence of a unique relation between energy and momentum, the spectral weight sum rule is now valid for all states at a given momentum but not for all states at a given energy, and there is no reason to expect the same power law behavior as that at low energies.

In this paper, we compute the edge spectral function from a microscopic approach using the method of CF diagonalization (CFD), wherein we consider a truncated basis of states that contain no pairs of electrons with angular momentum unity. These are the only states that survive when the Haldane pseudopotential[11,12] $V_1$ is taken to be infinitely strong; all states containing pairs with angular momenta equal to unity are pushed to infinity. Laughlin's 1/3 wave function[13] is exact for this model. Restriction to this subspace is also tantamount to considering edge excitations within the lowest $\Lambda$ level (or effective Landau level of composite fermions). A neglect of $\Lambda$ level mixing has been shown to be very accurate for the bulk physics, and we explicitly confirm below, by comparison to exact diagonalization results for small systems, that it provides a good first approximation for the edge excitations as well. Restricting to this truncated basis allows us to study systems with a large

 

number of particles, providing better thermodynamic estimates than were available previously.

We determine the thermodynamic limit of the dispersion of the elementary edge excitation. Our results show that while it is linear at low energies, it begins to deviate from linearity at an energy that is a fraction the 1/3 bulk gap. It also exhibits a roton minimum, which vanishes at a critical setback distance signaling edge reconstruction,[14] in agreement with previous work.[15,16] We show that while the spectral weights of individual excitations depend on various parameters,[16] they accurately obey the sum rule mentioned above over the entire parameter range that we have studied.

To determine the effect of the nonlinear dispersion on the edge exponent we employ a hybrid approach described in Sec. V, wherein we build the spectrum from the elementary edge boson with a nonlinear dispersion but assume the spectral weights of the EFTA model. We evaluate the tunneling *I-V* characteristic and find that the calculated exponent remains unchanged to a very good approximation even at energies above the edge roton energy where the dispersion is nonlinear. Zülicke and MacDonald[17] have also calculated the spectral function and the *I-V* characteristics for a $\nu=1/3$ edge by assuming a dispersion $\epsilon(q)\sim -q\ \ln(\alpha q)$ for the edge magnetoplasmon, where $q$ is the momentum and $\alpha$ is a constant; they have found that the edge exponent varies as the inverse filling. Our calculation is based on a magnetoplasmon dispersion that is obtained from a microscopic calculation for a system with Coulomb interaction and a realistic confinement potential. Recently, the effect of a nonlinearity of the fermionic spectrum on the long-distance, low-energy correlation functions has been studied in Refs. 18 and 19. However, this analysis considers a system in which both right- and left-moving modes are present and interact with each other, and it is not clear whether the same analysis would be applicable to a FQH edge with a single chiral mode.

One may also expect some signature in tunnel transport that may be associated with the edge roton, which would then allow such transport to serve as a spectroscopic probe of the edge roton. However we find that the effect of edge roton on tunnel transport is negligible because the spectral weight in the edge roton mode is very small.

Our paper is organized as follows. Section II contains a description of the model and the method of calculation. In Sec. III, we evaluate the energy spectra for small systems and compare them with the exact results. In Sec. IV, we study large systems and extract the thermodynamic edge dispersion, edge reconstruction, and edge roton. In Sec. V, we calculate the spectral weights and the associated sum rules for the EFTA, and we test the validity of these rules for the electronic spectra. We also outline our approach to calculate spectral function and tunneling density of states. In Sec. VI, we calculate the spectral function and tunneling density of states, present our main results on the *I-V* characteristics, and mention their implications for the robustness of the edge exponent under a nonlinear dispersion. In Sec. VII, we discuss a system with a reconstructed edge using a field-theoretic approach and address the effect of interaction between multiple bosons on the tunneling exponent. We conclude in Sec. VIII with a summary and a discussion of the causes and implications of our main results. In the Appendix we give a mathematical formalism for the spectral weights, sum rules, and the Green's functions for an ideal and a nonideal EFTA.

## II. MODEL AND METHOD OF CALCULATION

### A. Hamiltonian

We consider a two-dimensional electron system in a plane. The confinement is produced by a neutralizing background with uniformly distributed positive charge in a disk (denoted $\Omega_N$) of radius $R_N=(\sqrt{2N/\nu})l$; here $N$ is the number of electrons, $\nu$ is the filling factor, and $l=\sqrt{\hbar c/eB}$ is the magnetic length. (The symbol $l$ is also used for angular momentum later but the meaning ought to be clear from the context.) The background charge disk is separated from the electron disk by a setback distance $d$. The ground state of the electron is determined by a microscopic calculation; we expect the electrons to be approximately confined to a disk of radius $R_N$ to ensure charge neutrality in the interior. This system is modeled by the following Hamiltonian:

$$\begin{aligned} H &\equiv E_{\mathrm{K}} + V_{\mathrm{ee}} + V_{\mathrm{eb}} + V_{\mathrm{bb}} \\ &= \sum_j \frac{1}{2m_b}\left(\boldsymbol{p}_j + \frac{e}{c}\boldsymbol{A}_j\right)^2 + \sum_{j<k}\frac{e^2}{\epsilon|\boldsymbol{r}_j-\boldsymbol{r}_k|} \\ &\quad - \rho_0 \sum_j \int_{\Omega_N} d^2r \frac{e^2}{\epsilon\sqrt{|\boldsymbol{r}_j-\boldsymbol{r}|^2+d^2}} \\ &\quad + \rho_0^2 \int_{\Omega_N}\int_{\Omega_N} d^2r d^2r' \frac{e^2}{\epsilon|\boldsymbol{r}'-\boldsymbol{r}|}, \end{aligned} \tag{2}$$

where the terms on the right-hand side represent the kinetic, electron-electron, electron-background, and background-background energies, respectively. Here $m_b$ is the band mass of the electrons, $\boldsymbol{p}_j$ is the momentum operator of the $j$th electron and $\boldsymbol{r}_j$ is its position, $\boldsymbol{A}_j$ is the vector potential at $\boldsymbol{r}_j$, $\rho_0=\nu/2\pi l^2$ is the positive charge density spread over a disk of radius $R_N$, and $\epsilon$ is the dielectric constant of the background semiconductor material. At large magnetic fields, only the lowest Landau level states are occupied; hence the kinetic energy $\hbar\omega_c/2$ (where $\omega_c\equiv eB/m_bc$ is the cyclotron frequency) is a constant which will not be considered explicitly.

### B. Electron states

The single-particle states in the $n$th Landau level are given, in the symmetric gauge, by

$$\eta_{n,m}(z) = \frac{(-1)^n}{\sqrt{2\pi}}\sqrt{\frac{n!}{2^m(m+n)!}}e^{-r^2/4}z^m L_n^m\left(\frac{r^2}{2}\right), \tag{3}$$

where $L_n^m(x)$ is the associated Laguerre polynomial,[20] $n$ and $m$ denote the Landau level index and angular momentum index, respectively, $z=x-iy$ represents the electron coordinates in the complex plane, $r=|z|$, and all lengths are quoted in units of the magnetic length $l$. The lowest Landau level

states ($n=0$) are of special importance for our calculations below; they are given by

$$\eta_{0,m}(z) = \frac{z^m e^{-|z|^2/4}}{\sqrt{2\pi 2^m m!}}. \tag{4}$$

The many-body states are formed by taking linear combinations of antisymmetric products of single-particle wave functions denoted by $|p_1,p_2,\ldots,p_N\rangle = a^\dagger_{p_1} a^\dagger_{p_2}\cdots a^\dagger_{p_N}|0\rangle$, where $p_i=\{n_i,m_i\}$ is the single-particle state index of the $i$th electron and $a^\dagger_{p_i}$ is the corresponding creation operator. We will be interested in the edge excitations of the FQH state at $\nu=1/3$ below. The ground state has total angular momentum $M_0=3N(N-1)/2$. The angular momentum of the excited state, $\Delta M$, will be measured relative to $M_0$.

### C. Models of FQH edge

The tunneling of electrons from a two-dimensional electron gas into a Fermi liquid (such as a metal or $n+$ doped GaAs) has been studied experimentally in two geometries: point-contact geometry and cleaved-edge-overgrowth geometry.[8] These are believed to represent realizations of smooth and sharp edges, respectively.[21]

In the point-contact geometry, the boundary of the two-dimensional electron gas is smooth. Theoretically a smooth edge can be modeled by including all possible many-body edge excitations for a given total angular momentum $M$ $(=\Sigma_{i=1}^N m_i)$, placing no restrictions on the maximum single-particle angular momentum $m_i$. The smoothness is ensured by states extending a few magnetic lengths beyond the disk edge.

The cleaved-edge geometry is characterized by a long and thin tunneling barrier with a typical barrier width of about one magnetic length. Recent experiments suggest that the cleaved-edge overgrowth represents the realization of a sharp quantum Hall edge.[21] A sharp edge can be modeled[15] by excluding the single-particle angular momenta beyond a cutoff $m_{max}$, given by

$$m_{max} = 3(N-1) + l_0, \tag{5}$$

where $l_0$ is taken to be a small integer.

We have calculated the edge spectra for both smooth edge and sharp edge (the latter with cutoff $l_0=2$). We show in Sec. III that the low-energy branch of the sharp edge matches with that of the smooth edge, and hence the edge dispersion is not very sensitive to this issue. The calculations for the spectral functions are carried out for a smooth edge only. We note that a sharp edge eliminates several higher energy states but does not significantly affect the low-energy branch and hence edge reconstruction.

### D. Exact diagonalization

The exact interaction energy for FQH systems can be calculated for small systems using numerical diagonalization techniques. In the disk geometry with symmetric gauge, for a given total angular momentum $M$, the basis states $|m_1,m_2,\ldots,m_N\rangle$ in the lowest Landau level are generated according to the conditions,

$$\sum_j m_j = M; \quad 0 \le m_1 < m_2 \cdots < m_N. \tag{6}$$

Restricting to the lowest Landau level, the Hamiltonian in the second-quantized representation is

$$H = \frac{1}{2}\sum_{r,s,t,u} \langle r,s|V_{ee}|t,u\rangle a^\dagger_r a^\dagger_s a_t a_u + \sum_m \langle m|V_{eb}|m\rangle a^\dagger_m a_m + V_{bb}. \tag{7}$$

Here the electron-electron and electron-background interaction matrix elements are defined as

$$\langle r,s|V_{ee}|t,u\rangle = \int d^2r_1 d^2r_2\, \eta^*_r(r_1)\,\eta^*_s(r_2)\frac{e^2}{\epsilon r_{12}}\eta_t(r_1)\,\eta_u(r_2),$$

$$\langle m|V_{eb}|m\rangle = -\rho_0 \int d^2r_1 \int_{\Omega_N} d^2r_2 \frac{|\eta_m(r_1)|^2}{\sqrt{r_{12}^2+d^2}} \tag{8}$$

with $r+s=t+u$.

The background-background interaction energy per particle is calculated analytically to be

$$\frac{\langle V_{bb}\rangle}{N} = \frac{\rho_0^2}{2N}\int_{\Omega_N} d^2r \int_{\Omega_N} d^2r' \frac{e^2}{\epsilon|\boldsymbol{r}-\boldsymbol{r}'|} = \frac{8}{3\pi}\sqrt{\frac{\nu N}{2}} \tag{9}$$

with the energy measured in units of $e^2/\epsilon l$. This adds a constant term to the matrix elements of the Hamiltonian. (The constant background-background interaction must be included to obtain a sensible thermodynamic limit for the energy but is irrelevant for energy *differences*.) Computing the electron-background interaction $\langle V_{eb}\rangle$ requires numerical integration. To this end, we can write the electron-background energy as

$$V_{eb} = \sum_{i=1}^N v_{eb}(\boldsymbol{r}_i),$$

$$v_{eb}(\boldsymbol{r}_i) = -\rho_0 \int_{\Omega_N} d^2r \frac{e^2}{\epsilon\sqrt{|\boldsymbol{r}_i-\boldsymbol{r}|^2+d^2}} \equiv -\sqrt{2\nu N}F_b(r_i/R_N;d). \tag{10}$$

For $d=0$, the integral in Eq. (10) on the right-hand side can be calculated analytically, the result of which has been given by Ciftja and Wexler.[22] For $d\neq 0$, numerical integration is necessary. Figure 1 shows plots of the function $F_b$ for different $d$ and $N$.

For the electron-electron interaction, we find the analytical expressions for $\langle r,s|V_{ee}|t,u\rangle$ given by Tsiper in Ref. 23 to be useful. It is then straightforward to construct the Hamiltonian matrix and diagonalize it either by using standard diagonalization procedures for small systems ($N\le 7$) to get the full spectrum or by the Lanczos algorithm for slightly larger systems ($N=8,9$) to get the low-energy spectrum. In the present work, we have performed full diagonalization for systems with up to seven particles.

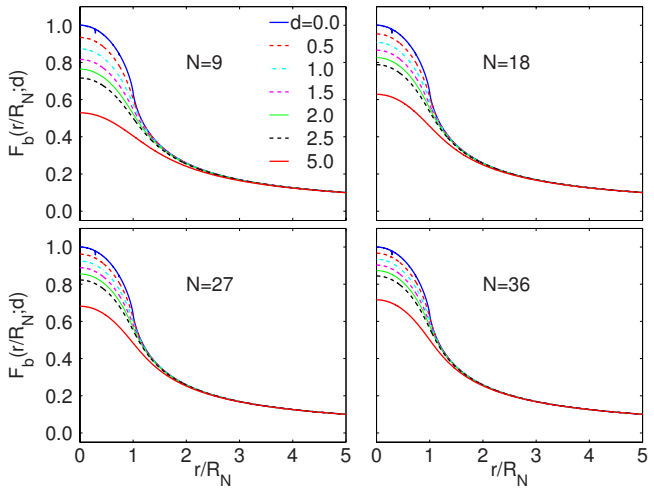


FIG. 1. (Color online) The function $F_b(r_i/R_N;d)$ that appears in the expression for the electron-background energy [Eq. (10)] for several values of $d$ and $N$. Here $r$ is the distance of the electron from the center of the disk and $R_N$ is the radius of the disk of the neutralizing positive background charge.

### E. CF diagonalization

We exploit the fact that the CF theory produces very accurate wave functions for low-energy eigenstates of the problem. Our approach will be to construct a truncated basis for the wave functions for the edge excitations,[12,24] and then diagonalize the full Hamiltonian within this basis to obtain various quantities of interest. The method has been described in detail in the literature,[9,25,26] so we present only a brief outline here.

For the fraction $\nu=n/(2np+1)$, the CF theory maps interacting electrons at total angular momentum $M$ to noninteracting composite fermions at $M^*=M-pN(N-1)$ (Refs. 27 and 28) by attaching $2p$ flux quantum to each electron. The ansatz wave functions $\Psi_\alpha^M$ for interacting electrons with angular momentum $M$ are expressed in terms of the known wave functions of noninteracting electrons $\Phi_\alpha^{M^*}$ at $M^*$ as follows:

$$\Psi_\alpha^M = \mathcal{P}_{\mathrm{LLL}} \prod_{j<k} (z_j - z_k)^{2p} \Phi_\alpha^{M^*}. \tag{11}$$

Here $\alpha=1,2,\ldots,D^*$ labels the different states, $\mathcal{P}_{\mathrm{LLL}}$ denotes projection into the lowest LL, and $D^*$ is the dimension of the CF basis. We choose $p=1$ as appropriate for $\nu=1/3$ and restrict $\Phi_\alpha^{M^*}$ to states with the lowest kinetic energy at $M^*$. No lowest Landau level projection is required for these states, as they are already in the lowest Landau level.

The Landau levels at $M^*$ transform into Landau like effective kinetic-energy levels of composite fermions, called $\Lambda$ levels. The restriction to the lowest Landau level at $M^*$ is equivalent to restricting composite fermions to their lowest $\Lambda$ level. More accurate spectra can be obtained by allowing $\Lambda$ level mixing and performing CFD in a larger space but that will not be pursued here. As will be seen below, the lowest $\Lambda$ level results are sufficiently accurate for our purposes.

The advantage of CF diagonalization is that the dimension $D^*$ of the CF basis is much smaller than the dimension of the full lowest Landau level Hilbert space at $M$; this allows a study of much larger systems. Table I compares the dimensions of the full Hilbert space ($D$) and the truncated CF space ($D^*$) for 6–12 particles for several values of $\Delta M$. The dimension $D$ increases exponentially, approximately as $D=10^{-2}\exp(2N)$ for large $N$. This gives $D\approx 2\times 10^{29}$ for $N=36$ particles, in dramatic contrast to $D^*\sim 10-100$ for $0\le\Delta M<10$. Of course, the Hilbert space reduction comes with a cost: the CF basis functions are much more complicated than the usual single Slater determinant basis functions, and diagonalization of the Hamiltonian in this basis requires many nontrivial steps and extensive Monte Carlo. Nonetheless, CF diagonalization can be, and has been, performed for many nontrivial cases of interest.

We need to evaluate the matrix elements of the Hamiltonian in our CF basis. If $\Psi_\alpha^M(z_1,z_2,\ldots,z_N)$ and $\Psi_\beta^M(z_1,z_2,\ldots,z_N)$ denote two CF states at angular momentum $M$, then the electron-background and electron-electron energy matrix elements are given by $\langle\Psi_\alpha^M|V_{\mathrm{eb}}|\Psi_\beta^M\rangle$ and $\langle\Psi_\alpha^M|V_{\mathrm{ee}}|\Psi_\beta^M\rangle$. Their evaluation requires evaluating multidi-

TABLE I. Dimension $D$ of the full Hilbert space (used in exact diagonalization) for several values of $N$ and $\Delta M$. Here $\Delta M$ is the angular momentum measured relative to the angular momentum $M_0=3N(N-1)/2$ of the ground state of the $\nu=1/3$ FQH state. The last column gives $D^*$, the dimension of the CF basis in the lowest $\Lambda$ level, used in our CF diagonalization. The values of $D^*$ are given for sufficiently large $N$ where they are $N$ independent; for small $N$, $D^*$ may be smaller than the given value.

| $\Delta M$ | $D(N=6)$ | $D(N=7)$ | $D(N=8)$ | $D(N=9)$ | $D(N=10)$ | $D(N=11)$ | $D(N=12)$ | $D^*$ |
|---|---|---|---|---|---|---|---|---|
| 0 | 1206 | 8033 | 55974 | 403016 | 2977866 | 22464381 | 172388026 | 1 |
| 1 | 1360 | 8946 | 61575 | 439100 | 3218412 | 24117499 | 184030746 | 1 |
| 2 | 1540 | 9953 | 67696 | 478025 | 3476314 | 25879361 | 196384297 | 2 |
| 3 | 1729 | 11044 | 74280 | 519880 | 3752096 | 27755663 | 209483911 | 3 |
| 4 | 1945 | 12241 | 81457 | 564945 | 4047402 | 29753578 | 223373383 | 5 |
| 5 | 2172 | 13534 | 89162 | 613331 | 4362833 | 31879397 | 238091562 | 7 |
| 6 | 2432 | 14950 | 97539 | 665355 | 4700201 | 34141000 | 253686437 | 11 |
| 7 | 2702 | 16475 | 106522 | 721125 | 5060174 | 36545347 | 270200645 | 15 |
| 8 | 3009 | 18138 | 116263 | 780997 | 5444732 | 39101065 | 287686698 | 22 |

mensional integrals, which can be effectively accomplished by Monte Carlo techniques described in the next section. The CF basis functions are in general not orthogonal to each other. They can be orthogonalized by the Gram-Schmidt procedure adapted for CF states to produce the energy spectrum as described in the literature.[9,12,25,26] Essentially, given the interaction matrix $\hat{V}_{\alpha,\beta}=\langle\Psi_\alpha|V|\Psi_\beta\rangle$ and the overlap matrix $\mathcal{O}_{\alpha,\beta}=\langle\Psi_\alpha|\Psi_\beta\rangle$, the energies and eigenvalues are obtained by diagonalizing the matrix $\mathcal{O}^{-1}\hat{V}$.

### F. Monte Carlo methods

Multidimensional integrals can be evaluated most effectively by the Metropolis-Hastings Monte Carlo (MHMC) algorithm.[29–31] For a discussion of the application of MHMC algorithm to quantum many-body systems, in particular, to quantum Hall systems, we refer the reader to Refs. 12 and 22. For our energy calculations, we find it sufficient to thermalize for 100 000 iterations and then average over about 10–20 million iterations for each angular momentum. For spectral weights calculations, about 200 million iterations are required for the eigenvector. These numbers do not vary significantly with $N$ in the range of our study ($N\leq 45$) but the computation time increases exponentially with $N$ and $\Delta M$, limiting our study to systems up to $N=45$ particles for the energy spectrum, and $N=27$ for spectral weights. The energies were calculated for $\Delta M=1-8$ and the spectral weights for $\Delta M=1-4$.

## III. SMALL SYSTEM STUDIES

The CFD approach has been well tested in the past for the *bulk* physics at various filling factors and has been shown to capture the behavior of FQH systems accurately. Before proceeding to larger systems, we first test the validity of the CFD approach for the edge excitations.

Using the CF diagonalization procedure outlined earlier, we compute the edge excitation spectra for the $\nu=1/3$ state for several parameters in the range $d=0-2.5l$ and $\Delta M=0-8$. Figures 2 and 3 show comparisons of the CFD spectra with the exact spectra for smooth and sharp edges (exact diagonalization is possible for slightly larger systems for a sharp edge because of the additional restriction on the Fock space), demonstrating that the CFD approach is essentially exact. For a sharp edge, we have chosen the value $l_0=2$ [cf. Eq. (5)]. The exact diagonalization results in Fig. 3 are taken from Wan *et al.*[15] Consistent with their conclusions, we find that edge reconstruction occurs for $d$ greater than a critical separation.

For small systems the results for sharp and smooth edges are not very different, as shown in Fig. 4; both show edge reconstruction for $d>1.5l$. For larger systems, as seen below, edge reconstruction occurs for larger $d$ for the sharp edge as expected.

We note that the exact spectrum has many more states than the CFD spectrum because the latter is restricted to the subspace of states spanning only the lowest $\Lambda$ level. The spectra for the sharp edge are even further curtailed due to the restriction on the largest single-particle angular momentum.

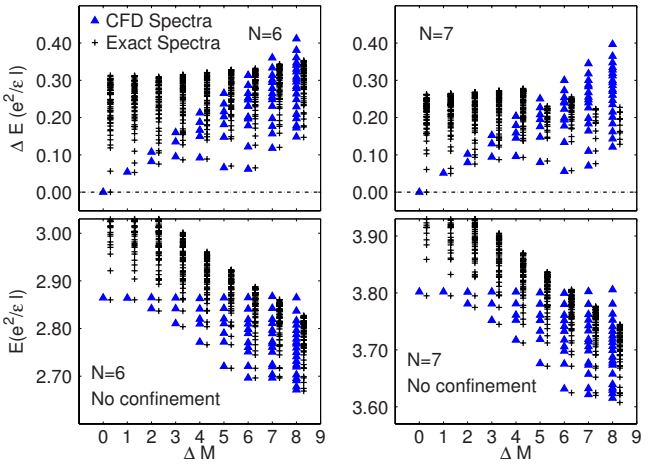


FIG. 2. (Color online) Comparison of CFD spectra with the exact spectra for the smooth edge for six and seven particles, with and without a positive background (upper panels and lower panels, respectively). For the upper panels, we have taken $d=0$. Blue triangles are the energies obtained by CF diagonalization and the adjacent "+" symbols (shifted along the $x$ axis for clarity) are the exact energies. The high-energy parts of the exact spectrum are not shown. All energies are quoted in units of $e^2/\epsilon l$ and are measured relative to the energy of the ground state at $\Delta M=0$. $\Delta M$ is the angular momentum of the excitation.

## IV. SPECTRA AND EDGE DISPERSION

Having ascertained the validity of our approach from comparisons to exact results, we now proceed to investigate the physics in the thermodynamic limit. We study the edge spectra for different sizes and approach the thermodynamic limit by identifying a scaling relation between the physical

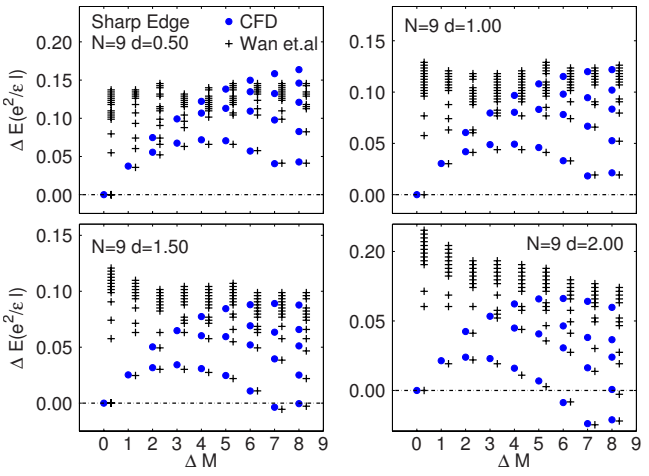


FIG. 3. (Color online) Comparison of the CFD spectra with the exact spectra for a sharp edge for $N=9$ particles at $\nu=1/3$ with $d=0.5-2.0l$. Blue dots indicate the energies obtained by CF diagonalization, whereas the adjacent + symbols (shifted along the $x$ axis for clarity) are energies extracted from the figures of Ref. 15.

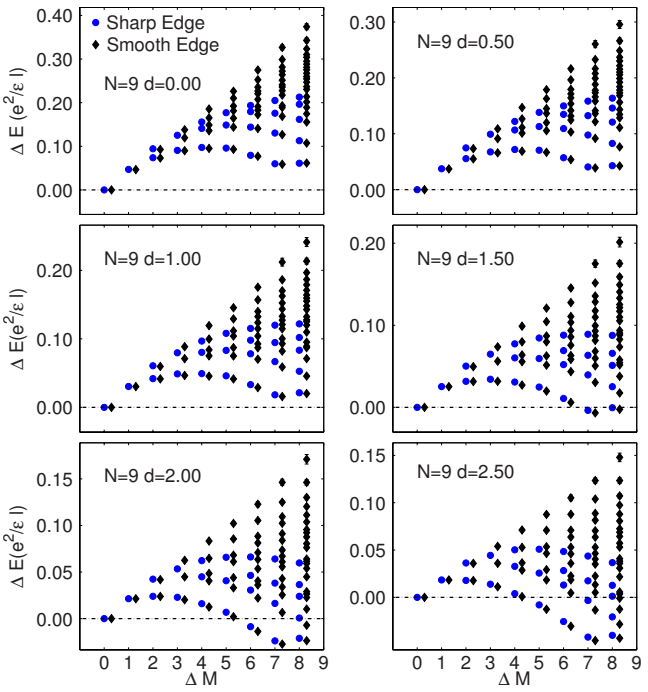


FIG. 4. (Color online) Energy spectra for smooth and sharp edge excitations of a $\nu=1/3$ system with $N=9$ and $d=0.0-2.5l$. Blue dots are for the sharp edge, whereas the adjacent black diamonds (shifted along the $x$ axis for clarity) are for the smooth edge.

momentum $\delta k$ (we take $\hbar=1$) and the edge angular momentum $\Delta M$. The momentum is related to the size of the system by $k \sim r/l^2$, where $r$ is the radius of the orbital wave function. For edge electrons, $r=\sqrt{2M}l=\sqrt{2[3(N-1)+\Delta M]}l$ for a system with $\nu=1/3$. This gives the momentum of the edge excitation to be

$$\delta k = \frac{\Delta M}{\sqrt{6(N-1)}l}. \tag{12}$$

Henceforth we will denote $\delta k$, the physical momentum of the edge excitation, as simply $k$. Based on our edge spectra results in Fig. 5, with the parameters $N=6-36$, $d=0-2.5l$, and $\Delta M=0-8$, we make the following observations.

(i) *Data collapse.* The energy spectra for different system sizes collapse, indicating proper scaling to the thermodynamic limit. The lowest branch in each of the four panels corresponds to the dispersion of the single edge boson, for various setback distances in the range $d=0-2.5l$. The data collapse to a single curve is apparent even for the second lowest branch, beyond which energies form a continuum. A few points for $N=36$ deviate slightly from the common trend in the lowest branch, which we believe is due to convergence problems for larger systems.

(ii) *Edge reconstruction.* For $d>d_c$, we observe edge reconstruction due to competing electron-background energy and electron-electron interaction energy.

(iii) *Nonlinearity and edge rotons.* The lowest branch, though linear at low $k$, eventually deviates from linearity for all $d$. We extract in detail the dispersion of the single boson excitation for various $d$ values in Fig. 6, with polynomial fits shown on the plots themselves. We observe that the edge dispersion is nonlinear and the "linearity breakdown"

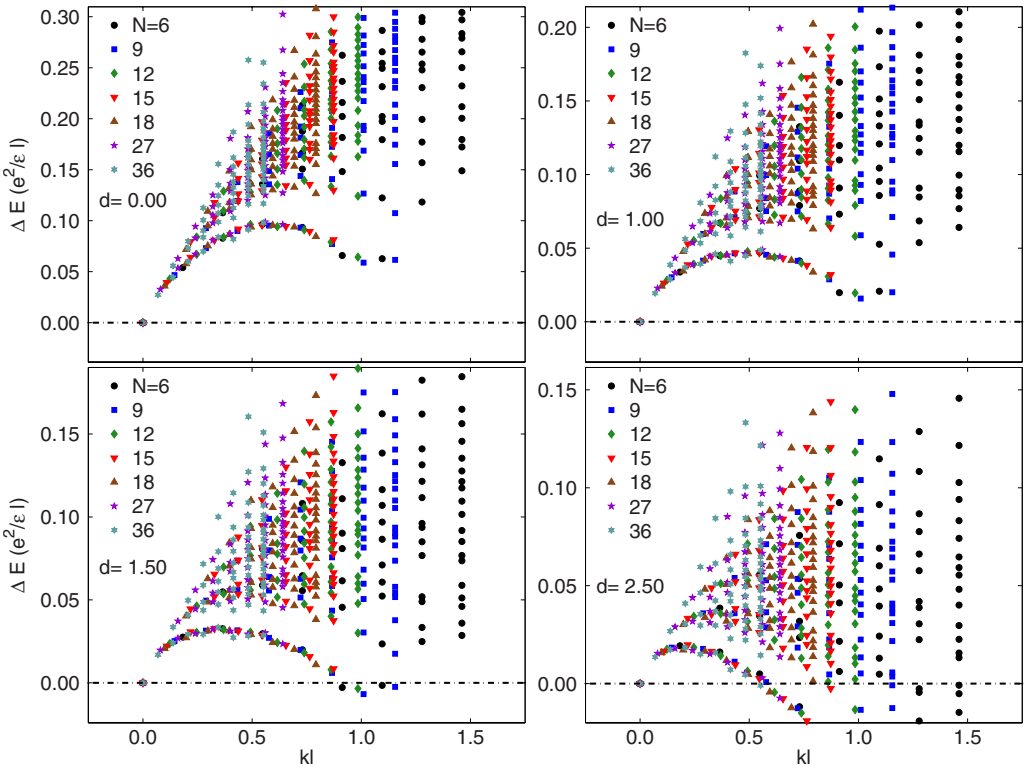


FIG. 5. (Color online) Edge spectra as a function of the physical momentum [see Eq. (12)] for $N=6-36$ particles. The setback distance $d=0.0-2.5l$. Data collapse for the lowest spectral branch can be seen in all the panels. Lower panels with $d \geq 1.5l$ show edge reconstruction.

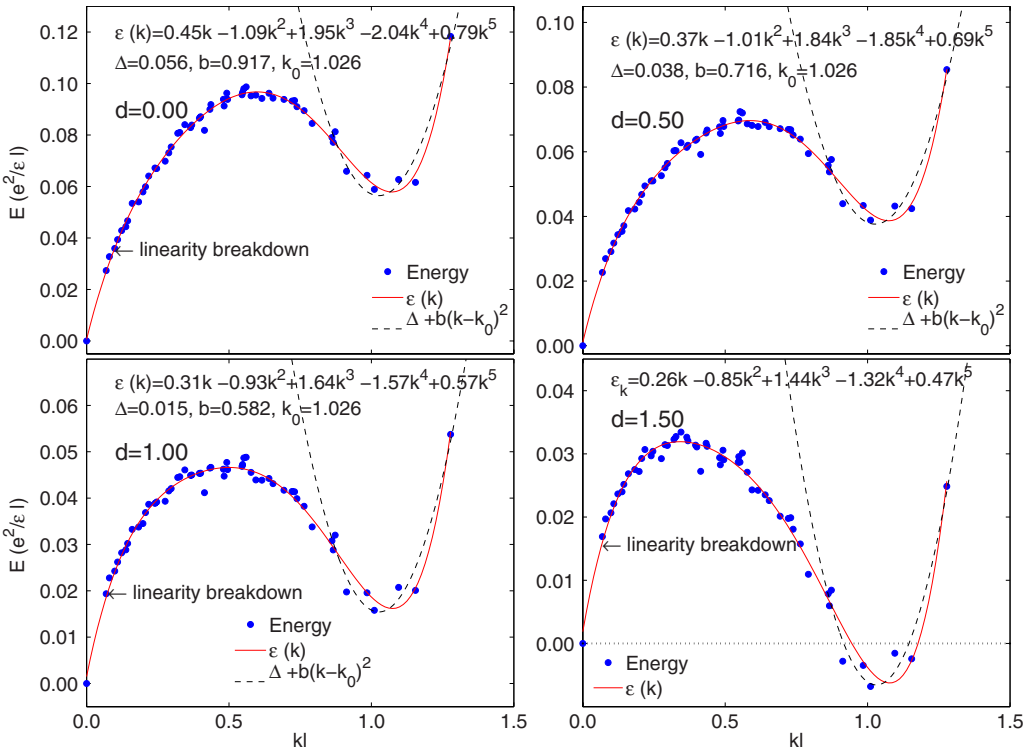


FIG. 6. (Color online) Dispersion $\epsilon(k)$ of single edge boson for different setback distances in the range $d=0-1.5l$. The solid lines are a fifth-order polynomial fit to the lowest branch of the energy spectra in Fig. 5. Arrows indicate the energy beyond which the dispersion becomes nonlinear, as defined in Sec. IV. Dispersion minima for the unreconstructed edges ($d<1.5l$) have been fitted with a roton curve $\epsilon_{\text{roton}}(k)=\Delta+b(k-k_0)^2$. Roton gap, momenta, and curvature corresponding to the roton minima are also shown. Note that Fig. 5 has $d$ up to $2.5l$ but in this figure we show the plots for the relevant distance range $d=0-1.5l$.

(defined as the point at which the deviation is ~20% from linear) occurs at energies in the range of $0.02-0.04(e^2/\epsilon l)$; in experiments in GaAs systems, this corresponds to the range 0.2–0.4 meV. For $d<d_c\approx 1.5l$, the dispersion also shows a roton structure with the minima around $k_0=1.026l^{-1}$. The roton gap $\Delta_R$ is approximately $0.056(e^2/\epsilon l)$ for zero setback distance but depends on the setback distance and collapses at approximately $d_c=1.5l$. The analytical fits for the dispersion relations are given in Fig. 6. For a different approach, see Ref. 32.

The nonlinear dispersion and the existence of the edge roton lie outside the assumptions of the EFTA model. In the next two sections we explore their effect on the edge exponent that is relevant to tunneling into the edge.

## V. BOSONIZATION OF FQH EDGE

The bosonic EFTA model is based on the idea that the edge excitations can be mapped into excitations of a bosonic system, given by

$$|\{n_l\}\rangle = \prod_{l=0}^{\infty} \frac{b_l^{n_l}}{\sqrt{n_l!}}|0\rangle, \tag{13}$$

where $n_l$ is the number of bosons in the orbital with angular momentum $l$. For a given state $\{n_l\}$, the total angular momentum and total energy are given by

$$\Delta M = \sum_l l n_l,$$

$$E_{\{n_l\}} = \sum_l n_l \epsilon_l. \tag{14}$$

Furthermore, the electron field operator at filling factor $\nu=1/m$ is given by[2]

$$\hat{\psi}^\dagger(\theta) \propto e^{-i\sqrt{m}\hat{\phi}(x)} = \sqrt{\eta} e^{-i\sqrt{m}\hat{\phi}_+(\theta)} e^{-i\sqrt{m}\hat{\phi}_-(\theta)}, \tag{15}$$

where $\sqrt{\eta}$ is a normalization factor. The fields $\hat{\phi}_+(\theta)$ and $\hat{\phi}_-(\theta)$ can be expanded in terms of bosonic creation and annihilation operators $b_l$ and $b_l^\dagger$ as

$$\hat{\phi}_+(\theta) = -\sum_{l>0} \frac{1}{\sqrt{l}} b_l^\dagger e^{il\theta},$$

$$\hat{\phi}_-(\theta) = -\sum_{l>0} \frac{1}{\sqrt{l}} b_l e^{-il\theta}. \tag{16}$$

### A. Electronic and Bosonic edge spectra

We first ask if the excitation spectrum of the electronic problem conforms to the bosonic prediction in which all excitations are created from a single branch of bosons. Following Ref. 15, we identify the lowest energy state at each an-

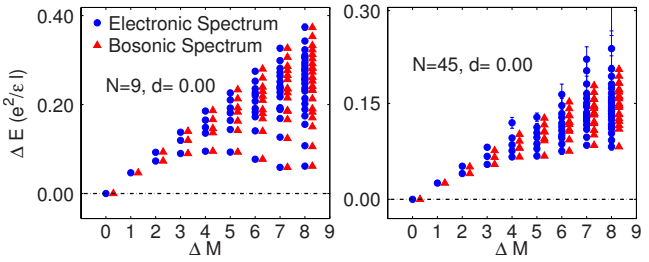


FIG. 7. (Color online) Energy spectrum for the edge excitations of $\nu=1/3$ (blue dots), obtained by CF diagonalization, for $N=9$ and 45 at $d=0.0$. Red triangles (shifted along the $x$ axis for clarity) show the bosonic spectra generated from its lowest branch (see Sec. V A for explanation).

gular momentum $\Delta M$ in the electronic spectrum with a single boson excitation at $l=\Delta M$, i.e., $n_l=\delta_{l,\Delta M}$. This gives the energy dispersion $\epsilon_l$ of the single boson state as a function of $l$, where we measure the energy $\epsilon_l$ with respect to the energy at $\Delta M=0$ ($M=M_0$). Using the equations $\Sigma_l l n_l=\Delta M$ and $E_{\{n_l\}}=\Sigma_l n_l \epsilon_l$, the energies of all the bosonic states $\{n_l\}$ can be obtained and identified with the energies of the corresponding electronic states. We note that in our truncated basis, the numbers of CF and bosonic states are equal at each $\Delta M$.

In Fig. 7, we compare the bosonic excitation spectrum obtained in this manner with the electronic spectra computed through CFD for the edges for the cases $N=9$ and 45 and $d=0.0$. The CFD spectra are shown in blue circles and the bosonic spectra are shown in red triangles. In all cases, the spectra obtained from the bosonic picture, with the single boson dispersion as an input, show a close resemblance to the electronic spectra, confirming the bosonic picture as well as the interpretation of the lowest branch as the single boson branch. (The bosonic description becomes less accurate with increasing $N$ or $\Delta M$ but still remains accurate for the low-energy states.)

### B. Spectral weights

The relation between the electron and the boson operators given in Wen's ansatz in Eq. (1) leads to a precise prediction for the matrix elements of the electron field operator. We will study, following Palacios and MacDonald (Ref. 10), these matrix elements, called spectral weights, defined by

$$C_{\{n_l\}} = \frac{\langle \{n_l\}|\hat{\psi}^\dagger(\theta)|0\rangle}{\langle 0|\hat{\psi}^\dagger(\theta)|0\rangle}, \tag{17}$$

where $|\{n_l\}\rangle$ represents the bosonic state with occupation $\{n_l\}$, $|0\rangle$ is the vacuum state with zero bosons, $\hat{\psi}^\dagger(\theta)$ is the electron creation operator at position $\theta$ (with one dimension wrapped into a circle), and $l$ denotes the single boson angular momentum.

Using Eqs. (1), (13), and (16), it is straightforward to obtain the EFTA predictions for the spectral weights

$$|C_{\{n_l\}}|^2 = \frac{m^{n_1+n_2+\cdots}}{n_1!n_2!\cdots 1^{n_1}2^{n_2}\cdots}. \tag{18}$$

We note that the denominator in Eq. (17) eliminates the unknown normalization constant $\sqrt{\eta}$ in Eq. (15).

To obtain the spectral weights from our electronic spectra, we need to identify a "dictionary" between the bosonic states and the electronic states. It is natural to identify the vacuum state $|0\rangle$ with the ground state of interacting electrons at $\nu=1/m$, denoted by $|\Psi_0^N\rangle$. The field operator has the standard meaning of

$$\hat{\psi}^\dagger(\theta) = \sum_l \eta_l^*(\theta) a_l^\dagger \equiv \sum_l \psi_l^\dagger(\theta), \tag{19}$$

where $a_l^\dagger$ and $a_l$ are the creation and annihilation operators for an electron in the angular momentum $l$ state, the wave function for which is given in Eq. (4). The wave function $\Psi_{\{n_l\}}^{N+1}(\{z_i\})$ is the electronic counterpart of the bosonic state $|\{n_l\}\rangle$ obtained through CF diagonalization. Using these definitions we calculate the electronic spectral weights. The details of the mapping and calculational method have been discussed in a previously published work.[16]

### C. Spectral weight sum rules

As seen below, a sum rule for the spectral weights plays an important role. For $\nu=1/m$, in the bosonic EFTA, the sum of the squared spectral weights (SSWs) is given by (see the Appendix for a derivation)

$$\mathrm{SSW}_{\Delta M}^{\mathrm{EFTA}} = \frac{(\Delta M+m-1)!}{\Delta M!(m-1)!},$$

$$\sum_l l n_l = \Delta M. \tag{20}$$

It is natural to ask whether the above relation holds for the real FQH edge. We test the validity of the sum rules for $\nu=1/3$ in our model of a FQH edge by computing the spectral weights for system sizes $N=9-27$ and $\Delta M=1-3$. The results for individual spectral weights have been published in a previous work by two of the authors.[16] In Fig. 8, we show the plots of the SSW for Coulomb interactions for different $N$. The thermodynamic limit for the SSW approaches the expected result according to Eq. (20).

### D. A hybrid model

To obtain results for the spectral function and the tunneling density of states in the parameter regime of our interest, bigger systems and larger angular momenta are needed. We have found that it is computationally infeasible to calculate the spectra for $N\gtrsim 50$ and $\Delta M\gtrsim 8$, and spectral weights for $N\gtrsim 27$ and $\Delta M\gtrsim 4$. Consequently, it is not possible to obtain tunneling $I$-$V$ from CF diagonalization. To make further progress we use a hybrid approach wherein we make the following assumptions: (i) the single boson dispersion is given by the microscopic CF diagonalization. (ii) The full spectrum can be constructed from it by assuming that the

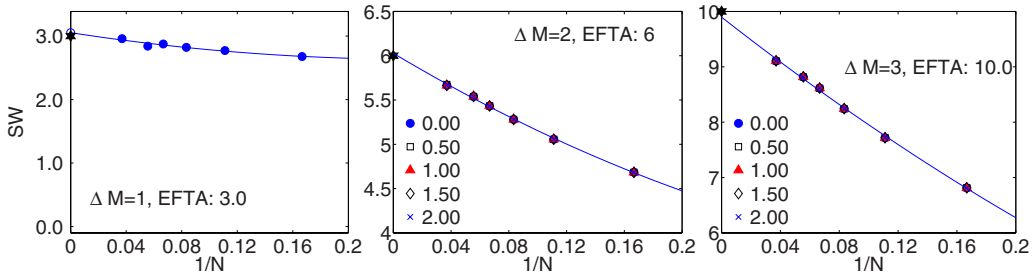


FIG. 8. (Color online) Sum of spectral weights [Eq. (18)] obtained from the electronic spectra (see Sec. V B for definition) at angular momenta $\Delta M=1-3$ and $d=0-2.0l$. For $\Delta M=1$, there is only one state, which is independent of $d$ in our model. For other cases we find that the spectral weight sum is independent of $d$. Also, the thermodynamic limit is consistent with the sum rule derived from the EFTA [see Eq. (20)].

bosons are noninteracting. (iii) Coupling to states outside our restricted basis can be neglected. (iv) The spectral weights of individual states are given by the EFTA model.

The assumption (i) is seen to be an excellent approximation for small systems, where exact results are available. The results in Fig. 5, which show that the single boson dispersion for different particle numbers collapses into a single curve, give us confidence that this is also a very good approximation for large systems. The assumption (ii) is also a rather good approximation at all energies for small systems as seen in Figs. 3, 4, and 7. For large systems the free boson model generally captures the overall shape of the full excitation band, as seen in Fig. 7(b), but the agreement worsens when it comes to the details of the low-energy states. However, as we see below, the tunnel transport is not particularly sensitive to the low-energy states. Coupling to states outside the lowest $\Lambda$ level was considered in Ref. 9, and found to affect the edge exponent, but are beyond the scope of our present study. Our most serious simplifying approximation is the last one; a previous work[16] by two of the present authors demonstrated that the individual spectral weights depend on the interaction and are not necessarily consistent with the EFTA model.

These approximations are necessary to make further progress. As a result, our study below will not test all aspects of the EFTA but we expect it to capture how nonlinearity of the edge boson dispersion affects the edge physics. In other words, we have made approximations that will provide results consistent with the EFTA at very low energies, where the edge dispersion is linear, and our aim will be to investigate in what way nonlinearity in the dispersion affects the behavior.

As an illustration of our hybrid approach, we have plotted in panel (c) of Fig. 9 the spectral weights of various excited states discussed in Sec. V A. The figure illustrates that the spectral weights corresponding to a given number of bosons have roughly the same energy, in agreement with previous work by Zülicke and MacDonald.[17]

## VI. SPECTRAL FUNCTION AND TUNNELING DENSITY OF STATES

The positive-energy part of the electron spectral function is given by[12,33]

$$A^{>}(k,E)=\sum_{\alpha}|\langle\alpha,N+1|c_k^{\dagger}|0,N\rangle|^2\delta(E-E_{\alpha}^{N+1}+E_0^N), \tag{21}$$

where $\alpha$ denotes many-body energy eigenstates, and $k$ and $c_k^{\dagger}$ denote the momentum (or any other) quantum number and the corresponding electron creation operator, respectively. For the FQH edge, if we restrict to the states in the lowest Landau level, $\Psi_{\{n_l\}}^{N+1}(\{z_i\})$ would correspond to $|\alpha,N+1\rangle$. Using the definition of the spectral weight, we can write the spectral function as

$$A^{>}(k,\epsilon)=\eta\sum_{\{n_l\}}|C_{\{n_l\}}|^2\delta(\epsilon-E_{\{n_l\}}^{N+1}),$$

$$\sum_l ln_l=\lambda^{-1}k, \tag{22}$$

where $|C_{\{n_l\}}|^2$ is the electronic spectral weight, $E_{\{n_l\}}^{N+1}$ is the energy of the electronic spectra measured from the ground state of $N+1$ particles, and $\epsilon$ is the energy of the edge excitation measured with respect to the chemical potential $\mu$. Here, $\eta$ is the normalization factor $|\langle 0|\hat{\psi}^{\dagger}(\theta)|0\rangle|^2$ in Eq. (17). We divide the energy into discrete bins $[\epsilon-\delta/2,\epsilon+\delta/2)$ of width $\delta$ and sum over the spectral weights for states with the corresponding energies and momentum $k$ to calculate $A(k,\epsilon)$. As discussed in Sec. V D, we have used the electronic energy dispersion and the bosonic spectral weights to calculate the spectral function.

In Fig. 9, panel (a), we show the energy spectra with spectral weights (colored) for bosonic states. The low-energy states have comparatively smaller weight. The spectral function $A(k,\epsilon)$ (unnormalized and in arbitrary units) for different momenta $k$ is shown in panel (b). In panel (d) we note that the energy corresponding to the maximum of spectral function closely follows the line of maximum energy for a given momenta.

### A. Tunneling density of states

When an electron tunnels between two weakly coupled systems (labeled $L,R$) with a chemical potential difference $eV$, the tunneling current can be shown to be (Refs. 12 and 33),

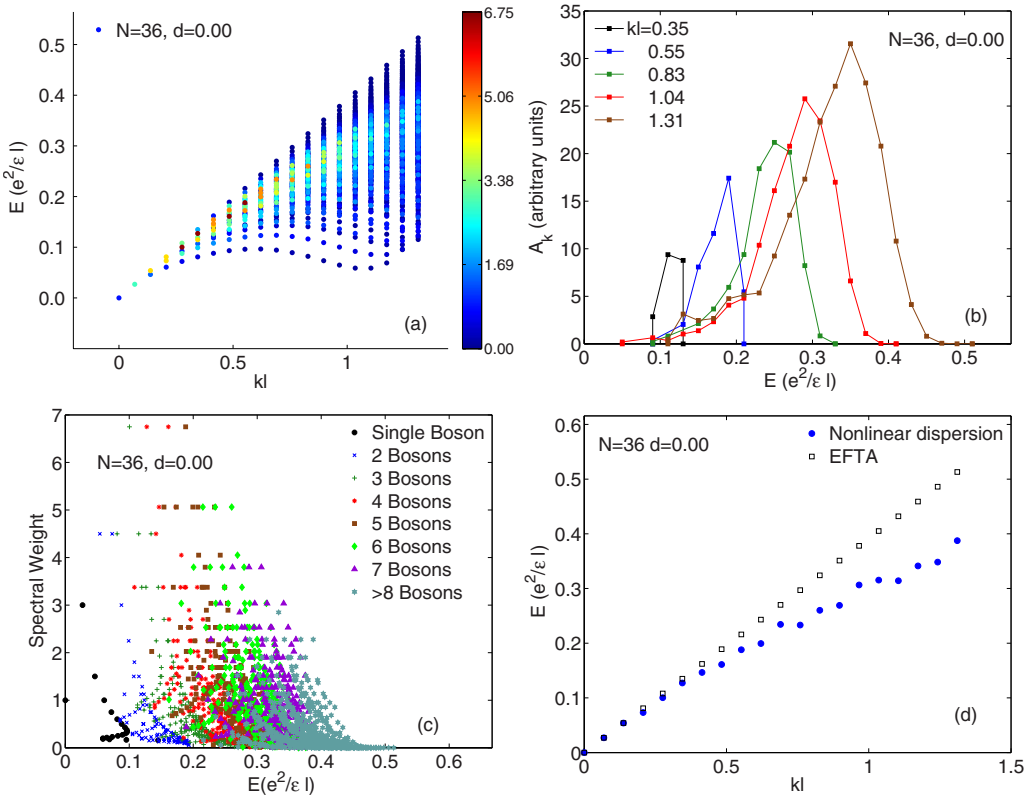


FIG. 9. (Color online) (a) Bosonic spectra generated through electronic dispersion for $N=36$ particles and $d=0.0$ using the hybrid approach described in Sec. V D; the bosonic spectral weights are shown in graduated colors. (b) Spectral function calculated from Eq. (22) for different $k$ using the data in panel (a). (c) Bosonic spectral weights plotted as a function of the energy, grouped by the number of bosons. (d) Energy at the maxima of the spectral function for different $k$. The black empty squares indicate the situation for a linear dispersion corresponding to EFTA. The system has $N=36$ particles; the setback distance is $d=0.0$; and we have restricted to angular momentum up to $\Delta M_{max}=19$.

$$I(eV) \sim \sum_{\alpha,\beta} |T_{\alpha,\beta}|^2 \int_0^{eV} dE A_L(\alpha,E) A_R(\beta,eV-E), \quad (23)$$

where $\alpha$ and $\beta$ are the quantum numbers of the electron states in the two systems and $T_{\alpha,\beta}$ is the matrix element connecting the two states. If the energy range of tunneling is small, $T_{\alpha,\beta}$ can be approximated by a constant $T$ independent of the quantum numbers. Further assuming one system (say $L$) is a metal, whose the density of states is almost constant near the Fermi surface, gives the differential conductance as proportional to the tunneling density of states in the other system ($R$, labeled as "edge") as

$$\left.\frac{dI}{dV}\right|_{\text{metal-edge}} \sim D_{\text{edge}}(eV) \equiv \sum_{\alpha} A(\alpha,E). \quad (24)$$

For a FQH edge, using Eq. (22), the tunneling density of states (the superscript $N+1$ is omitted for brevity) is given by

$$D_{\text{edge}}(\epsilon) \sim \sum_{\{n_l\}} |C_{\{n_l\}}|^2 \delta(\epsilon - E_{\{n_l\}}). \quad (25)$$

The relation between $I$ and $V$ is given by

$$I(eV) \sim \sum_k \int_0^{eV} d\epsilon A^{>}(k,\epsilon) \sim \int_0^{eV} d\epsilon \sum_{\{n_l\}} |C_{\{n_l\}}|^2 \delta(\epsilon - E_{\{n_l\}}), \quad (26)$$

which is essentially the sum over all the squared spectral weights of states with excitation energy $\epsilon < eV$ (Ref. 17).

In Fig. 10, we show the $I$-$V$ characteristics computed for a system of $N=75$ particles. Log-log plots in these panels show several plateaus and steps in the low-voltage region, which are purely due to the finite-size effect of summing over a discrete set of spectral weights (in the low-energy regime we have very few states in spite of the fairly large number of particles considered). We observe, surprisingly in view of the physics described in Sec. I that the exponent $\alpha$ in $I \sim V^{\alpha}$ remains very close to the ideal EFTA result of 3, within numerical errors. To explore the reasons behind the robustness of the edge exponent to nonlinearities in the dispersion, we have plotted the energy at the maxima of the spectral function $A(k,\epsilon)$ as a function of $k$ in panel (d) of Fig. 9. In the energy region of interest ($\epsilon \leq 0.2$), the peaks roughly follow the ideal EFTA line. The low-energy states near the lower edge of the dispersion have comparatively

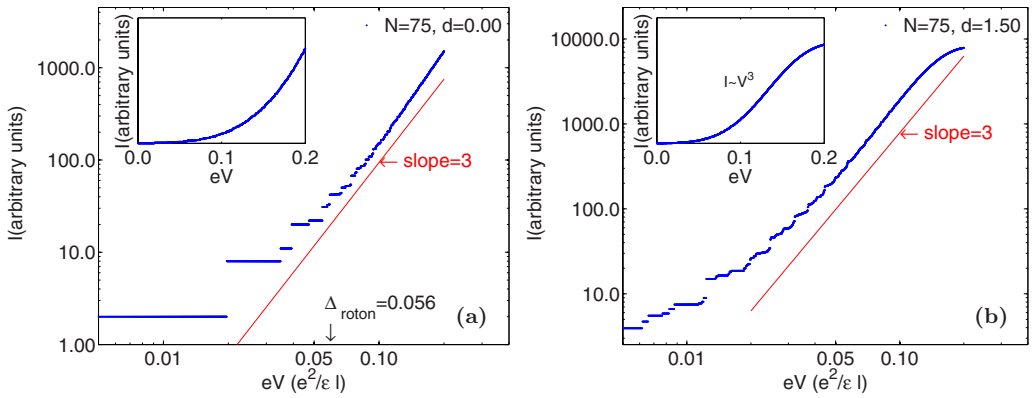


FIG. 10. (Color online) (a) The inset shows $I$ as a function of $V$ for tunnel transport between a FQH edge and a Fermi liquid computed from Eq. (26) using the numerical edge dispersion for $N=75$ particles. The main panel shows the log-log plot of $I$-$V$ characteristics to better bring out the power law behavior. The red line marks the curve $I \propto V^3$. The steplike deviations at small energies are a finite-size artifact (see text for explanation). A logarithmically small deviation can be seen at $eV=\Delta_{\text{roton}}$, the position of which has been marked. (b) Same as in panel (a) but for a setback distance where the roton gap $\Delta$ vanishes. The resulting slope is still close to 3 at energies $\epsilon<0.15$.

less spectral weight, and their contribution to the tunneling density of states is negligible.

### B. Irrelevance of edge roton in tunneling

One might ask whether the edge roton produces any signature in a tunneling experiment. In panel (a) of Fig. 10, no significant structure is seen when $eV$ is equal to the roton energy. Panel (b) corresponds to the setback distance where the roton gap just vanishes. Again, there is no prominently visible structure that may be attributed to the roton energy. An increase in the density of states at very low energies, shown in the log-log plots, is associated with the edge roton but such a signature would be difficult to detect in experiments. We surmise that the spectral weight in the roton mode is too small for it to be observable in tunnel transport.

## VII. EFFECTIVE APPROACH FOR RECONSTRUCTED EDGE AND TUNNELING EXPONENT

For systems which undergo edge reconstruction (in our case $d>d_c$), a logical procedure would be to study the excitations around the *new* ground state which now occurs at a finite $\Delta M$. This, however, is not possible in our numerical calculations because of computational limitations. For example, in the 27- or 45-particle system, we cannot go to large enough values of $\Delta M$ to identify the minimum energy.

To make further progress, we make the assumption that the edge-reconstructed system can be described by multiple chiral edges (we take three chiral edges below), which interact with one another. For want of a better description, we further assume that each chiral edge can be modeled by the EFTA Lagrangian and ask to what extent this can describe the experiments. We will use the technique of bosonization to study the effects of density-density interactions between three chiral modes; our notation and analysis will follow Chamon and Wen's theory of edge reconstruction.[14] A model with three modes (two of them moving in one direction and the other mode moving in the opposite direction) is motivated by the analysis of Yang[34] and Orgad.[35] We denote the modes as 1, 2, and 3, of which 1 and 3 move to the right and 2 moves to the left. We take the bosonic Lagrangian for the system to be of the form (we use a slightly different normalization for the bosonic field in this section than in Sec. V),

$$L = -\frac{1}{4\pi}\int_{-\infty}^{\infty} dx \left[ \sum_{p,q=1}^{3} \partial_t \phi_p K_{pq} \partial_x \phi_q + \sum_{p,q=1}^{3} \partial_x \phi_p V_{pq} \partial_x \phi_q \right], \tag{27}$$

where $K_{pq}$ is a diagonal matrix with entries given by $(1,-1,1)$, and $V_{pq}$ is a real symmetric matrix whose entries give the strengths of the interactions between pairs of edges. Note that with our convention, the filling factors $\nu_p$ $(p=1,2,3)$ do not appear in the Lagrangian in Eq. (27) but in the electron creation operator below.

In the absence of interactions between different edges (i.e., $V_{pq}=0$ if $p \neq q$), the velocities of the three modes are given by the diagonal entries, $v_p=V_{pp}$. When interactions between different edges are present, the Lagrangian in Eq. (27) can be diagonalized by doing a Bogoliubov transformation[14,36] to a new set of fields given by $\tilde{\phi}_p=\Sigma_q U_{pq}\phi_q$, where $U$ satisfies

$$(U^T)^{-1} K U^{-1} = K,$$

$$(U^T)^{-1} V U^{-1} = \tilde{V},$$

$$U^{-1} = K U^T K \tag{28}$$

with $\tilde{V}$ being a diagonal matrix whose entries give the velocities $\tilde{v}_p$ of the fields $\tilde{\phi}_p$.

Let us now consider a general electron creation operator of the form[14]

$$\psi(l_1,l_2,l_3) = \exp\left[ i \sum_p l_p \phi_p / \sqrt{\nu_p} \right], \tag{29}$$

where we have assumed that edge $p$ corresponds to filling fraction $\nu_p$. The operator in Eq. (29) creates $l_1$ and $l_3$ electrons on edges 1 and 3, respectively, and annihilates $l_2$

(or creates $-l_2$) electrons on edge 2; hence we must have $l_1-l_2+l_3=1$ in order that the operator should create one electron. Let us now assume that all the $\nu_p$ are equal to 1/3. In the case of no interactions ($V_{pq}=0$ for $p\neq q$), the operators with the smallest scaling dimension correspond to $(l_1,l_2,l_3)=(1,0,0)$, $(0,-1,0)$, and $(0,0,1)$; they all have scaling dimension equal to 3/2. If a weak interaction is now turned on between the counter-propagating edge 2 and the other two edges, the above scaling dimensions necessarily become larger than 3/2. For instance, the scaling dimension of the operator corresponding to (1,0,0) is given by

$$\frac{3}{2}[(U_{11})^2+(U_{21})^2+(U_{31})^2]. \tag{30}$$

Since the first equation in Eq. (28) implies that $(U_{11})^2-(U_{21})^2+(U_{31})^2=1$, the expression in Eq. (30) is larger than 3/2 if $U_{21}\neq 0$, i.e., if there is a nonzero interaction $K_{12}$ between modes 1 and 2. On the other hand, for long-range and strong Coulomb interactions, we have $V_{pq}=v_p\delta_{pq}+c$, where $c\gg v_p$.[14] For $c=\infty$, the operator with the smallest scaling dimension corresponds to (1,1,1) and has scaling dimension 3/2. Once again, if $c$ is large but finite, we find that this operator has a scaling dimension larger than 3/2; if all the $v_p$ are equal to $v$ and $v/c\ll 1$, we find that the scaling dimension is given by $(3/2)(1+16v^2/c^2)$. We thus see, in this model, that any interaction, weak or strong, between counter-propagating modes makes the scaling dimensions of all possible electron operators larger than 3/2; hence the exponent for the two-point correlation function for electrons becomes larger than 3. This result is inconsistent with the tunneling experiments[4–6,8] which measure an exponent of about 2.7. (We note, however, that the exponent is sample dependent, and in the experiment by Hilke *et al.*[7] an extrapolation of their results produces an exponent larger than 3 at $\nu=1/3$.) Wan *et al.*[15] and Joglekar *et al.*[37] also studied the reconstruction of FQH edges at $\nu=1/3$ and showed that the presence of counter-propagating edges leads to a nonuniversal exponent. Yang[34] introduced an action which has cubic and quartic terms in bosonic fields and showed that this also leads to an exponent slightly larger than 3. (In contrast, we have considered a standard action that is quadratic in the bosonic fields.)

## VIII. DISCUSSION AND CONCLUSIONS

We have investigated the influence of nonlinear dispersion on the physics of the FQH edge at $\nu=1/3$. Our approach involves microscopic calculations of the edge dispersion and the associated bosonic spectra, and the use of spectral weights from the bosonic theory.

The conclusions of our work are as follows. (i) The edge dispersion is linear for energies below $0.02-0.04e^2/\epsilon l$ (0.2–0.4 meV) depending on the electron-background separation. For $d<d_c=1.5l$, an edge magnetoroton is observed. The maximum roton gap is $\Delta\approx 0.056(e^2/\epsilon l)$ for zero setback distance.

(ii) Edge reconstruction occurs beyond a critical electron-background separation $d_c\approx 1.5l$ for smooth edges of a $\nu=1/3$ system, in agreement with the previous literature.[15]

(iii) A bosonic description of the edge excitation spectrum is satisfactory. It requires the dispersion of the single boson excitation as an input.

(iv) The spectral weights of the electronic dispersion, though individually different from that of predictions of the bosonic theory, obey the same sum rules for a given angular momentum (provided $\Lambda$ level mixing is neglected).

(v) The tunneling exponent is surprisingly insensitive to the nonlinearity in the edge boson dispersion. The peaks of the spectral function for different momenta roughly follow the linearity of the ideal EFTA. The low-energy states have a small spectral weights and contribute negligibly to the tunneling.

(vi) The roton has no significant contribution to the spectral function and hence to the tunneling density of states. Only a logarithmically weak signature of the roton may be observed in tunneling experiments.

(vii) It is well known that the model assuming a single chiral mode is not adequate for understanding the results of experiments on systems which undergo edge reconstruction. An effective theory description with three chiral edges at $\nu=1/3$ produces an exponent that is larger than 3, contrary to the experimental finding of a smaller-than-3 exponent.

We stress that some of these conclusions [such as (v) and (vi)] refer only to the effect of the nonlinearity of the edge dispersion. Other assumptions made in our study, such as our use of a restricted basis and of the EFTA spectral weights, may provide a further source of correction but these are beyond our present study.

## ACKNOWLEDGMENTS

We acknowledge Paul Lammert, Chuntai Shi, Sreejith Ganesh Jaya, and Vikas Argod for insightful discussions, support with numerical codes, and cluster computing. The computational work was done on the LION-XC/XO and *Hammer* cluster of the High Performance Computing (HPC) group, The Pennsylvania State University.

## APPENDIX

### 1. Sum rules

The derivation of the sum rules in Eq. (20) for squared spectral weights at a given angular momenta $\Sigma_{\{n_l\}}ln_l=M$ is given below. Consider the multinomial expansion (Ref. 20, p. 823)

$$\left(\sum_{k=1}^{\infty}\frac{x_k t^k}{k}\right)^m = m!\sum_{n=m}^{\infty}\sum_{\{a_j\}}\frac{t^n}{n!}\frac{n!\prod_i x_i^{a_i}}{\prod_j (a_j!j^{a_j})},$$

$$\sum_j ja_j=n,\quad \sum_j a_j=m. \tag{A1}$$

With the following transformations

$$m \to b \quad \text{number of bosons},$$

$$x_k \to m \quad \text{inverse filling factor},$$

$$a_j \to n_j \quad \text{bosons occupation},$$

$$n \to M \quad \text{angular momentum},$$

we obtain

$$\left(\sum_{k=1}^{\infty} \frac{mt^k}{k}\right)^b = b! \sum_{M=b}^{\infty} \sum_{\{n_j\}} \frac{t^M}{M!} \frac{M! \prod_i m^{n_i}}{\prod_j (n_j! j^{n_j})},$$

$$\sum_j j n_j = M,$$

$$\sum_j n_j = b. \tag{A2}$$

Hence we get

$$\sum_{b=0}^{\infty} \left(\frac{1}{b!} \sum_{k=1}^{\infty} \frac{mt^k}{k}\right)^b = \sum_{b=0}^{\infty} \sum_{M=b}^{\infty} \sum_{\{n_j\}} t^M \prod_j \frac{m^{n_i}}{n_j! j^{n_j}}. \tag{A3}$$

We simplify this by noting the relation

$$\exp\left(m \sum_{k=1}^{\infty} \frac{t^k}{k}\right) = e^{-m \ln(1-t)} = \frac{1}{(1-t)^m}. \tag{A4}$$

The sum of the squared spectral weights[10] is the coefficient of $t^M$

$$\sum_{\{n_l\}} |C_{\{n_l\}}^{(m)}|^2 = \frac{(M+m-1)!}{M!(m-1)!}, \quad \sum_l l n_l = M. \tag{A5}$$

### 2. Green's function

The ideal EFTA assumes a linear dispersion $\epsilon(k) = v_F k$ and the sum rule in Eq. (A5). The Green's function for the one-dimensional chiral edge is

$$G(x,t) = \langle 0 | T[\Psi(x,t)\Psi^\dagger(0,0)] | 0 \rangle$$
$$= \langle 0 | e^{-iHt} e^{ik0} \Psi(0,0) e^{-ikx} e^{iHt} \Psi^\dagger(0,0) | 0 \rangle, \quad t > 0. \tag{A6}$$

We map the edge to a disk by setting $x = R\theta$ with radius $R=1$ and insert a complete set of states within the subspace of single boson modes,

$$\sum_M \sum_{\{n_l\}} |M, \{n_l\}\rangle \langle M, \{n_l\}| = I_s; \quad M = \sum_l l n_l. \tag{A7}$$

We make the following substitutions:

$$k = \lambda M; \quad \lambda = M/\sqrt{6(N-1)},$$

$$\epsilon_{\{n_l\}} = \sum_l \epsilon_l n_l = \lambda v_F \sum_l l n_l = \lambda v_F M, \tag{A8}$$

and proceed to calculate the Green's function,

$$G(x,t) = \sum_M \sum_{\{n_l\}} e^{-ikx} \langle 0 | \Psi(0,0) e^{iHt} | M, \{n_l\} \rangle \langle M, \{n_l\} | \Psi^\dagger(0,0) | 0 \rangle$$
$$= \sum_M \sum_{\{n_l\}} e^{-i\lambda M(x - v_F t)} \langle M, \{n_l\} | \Psi^\dagger(0,0) | 0 \rangle |^2$$
$$= \sum_M e^{-i\lambda M(x - v_F t)} \sum_{\{n_l\}} |\langle M, \{n_l\} | \Psi^\dagger(0,0) | 0 \rangle|^2$$
$$= \sum_M e^{-i\lambda M(x - v_F t)} \binom{M+m-1}{m-1}$$
$$\sim \frac{1}{(x - v_F t)^m}. \tag{A9}$$

This shows how the power law follows from a combination of the linear dispersion and the sum rule. For a general dispersion $\omega_k$, we evaluate the commutators of the bosonic fields to find the Green's function for the edge,

$$G(x,t) = \frac{2\pi}{L} e^{m \Sigma_k (1/k) e^{-i(kx - \omega_k t)} e^{-ak}}. \tag{A10}$$


[1] D. C. Tsui, H. L. Stormer, and A. C. Gossard, Phys. Rev. Lett. **48**, 1559 (1982).
[2] X. G. Wen, Int. J. Mod. Phys. B **6**, 1711 (1992).
[3] X. G. Wen, Phys. Rev. Lett. **64**, 2206 (1990).
[4] A. M. Chang, L. N. Pfeiffer, and K. W. West, Phys. Rev. Lett. **77**, 2538 (1996).
[5] M. Grayson, D. C. Tsui, L. N. Pfeiffer, K. W. West, and A. M. Chang, Phys. Rev. Lett. **80**, 1062 (1998).
[6] A. M. Chang, M. K. Wu, C. C. Chi, L. N. Pfeiffer, and K. W. West, Phys. Rev. Lett. **86**, 143 (2001).
[7] M. Hilke, D. C. Tsui, M. Grayson, L. N. Pfeiffer, and K. W. West, Phys. Rev. Lett. **87**, 186806 (2001).
[8] A. M. Chang, Rev. Mod. Phys. **75**, 1449 (2003); M. Grayson, Solid State Commun. **140**, 66 (2006).
[9] S. S. Mandal and J. K. Jain, Solid State Commun. **118**, 503 (2001); Phys. Rev. Lett. **89**, 096801 (2002).
[10] J. J. Palacios and A. H. MacDonald, Phys. Rev. Lett. **76**, 118 (1996).
[11] F. D. M. Haldane, Phys. Rev. Lett. **51**, 605 (1983).
[12] J. K. Jain, *Composite Fermions* (Cambridge University Press, Cambridge, 2007).
[13] R. B. Laughlin, Phys. Rev. Lett. **50**, 1395 (1983).
[14] C. de C. Chamon and X. G. Wen, Phys. Rev. B **49**, 8227 (1994).
[15] X. Wan, E. H. Rezayi, and K. Yang, Phys. Rev. B **68**, 125307 (2003); X. Wan, K. Yang, and E. H. Rezayi, Phys. Rev. Lett. **88**, 056802 (2002).
[16] S. Jolad and J. K. Jain, Phys. Rev. Lett. **102**, 116801 (2009).
[17] U. Zülicke and A. H. MacDonald, Phys. Rev. B **54**, R8349 (1996).
[18] A. Imambekov and L. I. Glazman, Science **323**, 228 (2009).

[19] A. Imambekov and L. I. Glazman, Phys. Rev. Lett. **102**, 126405 (2009).
[20] M. Abramowitz and I. A. Stegun, *Handbook of Mathematical Functions* (Dover, New York, 1972).
[21] M. Grayson, M. Huber, M. Rother, W. Biberacher, W. Wegscheider, M. Bichler, and G. Abstreiter, Physica E **25**, 212 (2004).
[22] O. Ciftja and C. Wexler, Phys. Rev. B **67**, 075304 (2003).
[23] E. V. Tsiper, J. Math. Phys. **43**, 1664 (2002).
[24] J. K. Jain, Phys. Rev. Lett. **63**, 199 (1989).
[25] G. S. Jeon, C.-C. Chang, and J. K. Jain, Eur. Phys. J. B **55**, 271 (2007).
[26] J. K. Jain and R. K. Kamilla, Int. J. Mod. Phys. B **11**, 2621 (1997).
[27] G. Dev and J. K. Jain, Phys. Rev. B **45**, 1223 (1992).
[28] J. K. Jain and T. Kawamura, Europhys. Lett. **29**, 321 (1995).
[29] N. Metropolis, A. W. Rosenbluth, M. N. Rosenbluth, A. M. Teller, and E. Teller, J. Chem. Phys. **21**, 1087 (1953).
[30] W. K. Hastings, Biometrika **57**, 97 (1970).
[31] S. Chib and E. Greenberg, Am. Stat. **49**, 327 (1995).
[32] H. K. Nguyen, Y. N. Joglekar, and G. Murthy, Phys. Rev. B **70**, 035324 (2004).
[33] For reviews, see: G. D. Mahan, *Many Particle Physics*, 3rd ed. (Plenum, New York, 2000); G. F. Giuliani and G. Vignale, *Quantum Theory of Electron Liquid* (Cambridge University Press, Cambridge, 2005).
[34] K. Yang, Phys. Rev. Lett. **91**, 036802 (2003).
[35] D. Orgad and O. Agam, Phys. Rev. Lett. **100**, 156802 (2008).
[36] C. Tsallis, J. Math. Phys. **19**, 277 (1978).
[37] Y. N. Joglekar, H. K. Nguyen, and G. Murthy, Phys. Rev. B **68**, 035332 (2003).